JACS
JOURNAL OF THE AMERICAN CHEMICAL SOCIETY

Subscriber access provided by American Chemical Society

Article

Phospholipid Tubelets

Bijaya K. Mishra, Colleen C. Garrett, and Britt N. Thomas

J. Am. Chem. Soc., **2005**, 127 (12), 4254-4259• DOI: 10.1021/ja040191w • Publication Date (Web): 05 March 2005

Downloaded from http://pubs.acs.org on March 24, 2009

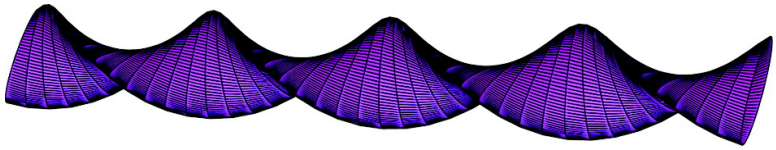

More About This Article

Additional resources and features associated with this article are available within the HTML version:

- Supporting Information
- Links to the 1 articles that cite this article, as of the time of this article download
- Access to high resolution figures
- Links to articles and content related to this article
- Copyright permission to reproduce figures and/or text from this article

View the Full Text HTML

ACS Publications
High quality. High impact.

Journal of the American Chemical Society is published by the American Chemical Society. 1155 Sixteenth Street N.W., Washington, DC 20036

J|A|C|S
ARTICLES
Published on Web 03/05/2005

Phospholipid Tubelets

Bijaya K. Mishra, Colleen C. Garrett, and Britt N. Thomas*

Contribution from the Department of Chemistry, Louisiana State University, Baton Rouge, Louisiana 70803

Received August 2, 2004; E-mail: bthomas@lsu.edu

Abstract: A novel electron microscopy specimen protocol shows that the presumed phospholipid bilayer membrane ribbons that wind helically to form the cylinders known as "tubules" are actually flattened tubes. These flattened tubes are alternatively found with a helical twist about the tube's long axis or occasionally flat with no winding or twist. Flat, cylindrically wound and axially twisted segments are routinely found along a single tube's length, and at the helically wound and axially twisted segment junctions, the chiral sense of the structure often, but not always, changes chiral sense.

1. Introduction

The phosphatidylcholine 1,2-bis(10,12-tricosadiynoyl)*sn*-glycero-3-phosphocholine [DC(8,9)PC] (compound **1** of Figure 1) and related diynoic lipids self-assemble in ethanolic solutions to form microscopic ($\sim$0.5 μm $\times$ $\sim$30 μm) hollow cylinders that possess an exterior helical trace, reminiscent of that found on a paper drinking straw. This feature makes evident that tubules form through the helical winding of a flat ribbon of width $\sim$0.5 μm and length $\sim$100 μm. Because phospholipid bilayer membranes are stabilized through the shielding of the phospholipids' hydrophobic tails from the aqueous environment, the exposed hydrocarbon tail found at the edge of an $\sim$200:1 aspect-ratio ribbon is difficult to reconcile.[1] Additional theoretical challenges in describing tubule formation and structure are presented by the diverse physical processes by which tubules form: (1) emergence from spherical L_α-phase vesicles; (2) directly from cooling solution, presumably via first-order crystallization; and (3) a process resembling one proposed in 1996 by Selinger and MacKintosh[5] that involves large ($\sim$100 μm $\times$ 300 μm) flat lamellar sheets shedding 1-μm-wide ribbons that wind helically into cylinders. This mechanism will be described fully in a forthcoming manuscript.[6] The conversion of L_α-phase spherical vesicles to L_β'-phase tubules is the preponderant tubule formation mechanism.

In this process, the ribbonlike structure emerges from the spherical L_α-phase vesicle in a helically coiled fashion, and the ribbon slowly widens until its opposing edges meet to form a continuous cylinder. While this closure presumably eliminates exposure of the ribbon's edges to the aqueous environment and the corresponding energetics expense, the persistence of the helical ridge makes clear that these edges do not fuse. This may be a consequence of the helical ribbon's nonfluid, chain-frozen L_β' state. But, several tubule-forming systems are known where helically wound ribbons' opposing long edges do *not* meet; for example, a significant proportion of DC(8,9)PC microstructures made in solutions where 2-propanol is substituted for ethanol contains "open" helices,[2] and approximately 10% of the tubules made from the phosphonate DC(8,9)PC derivatives of Figure 1 are similarly open under conditions where all DC(8,9)PC microstructures are closed cylinders. Open helical structures are found to persist in other unrelated aqueous tubule-forming systems.[3,4] Because amphiphilic structure formation is driven largely by minimizing hydrocarbon tail and water interaction, the extensive tail exposure that occurs along the presumed ribbon edge is problematic in reconciling the stability of open helices, and even of the transient helices destined to become tubules.

SAXS probes of the various structures resulting from the different molecules of Figure 1 show that interlamellar spacing is a tightly conserved quantity. The two DC(8,9)PC phosphonate derivatives of Figure 1, for example, make tubules whose 1-μm

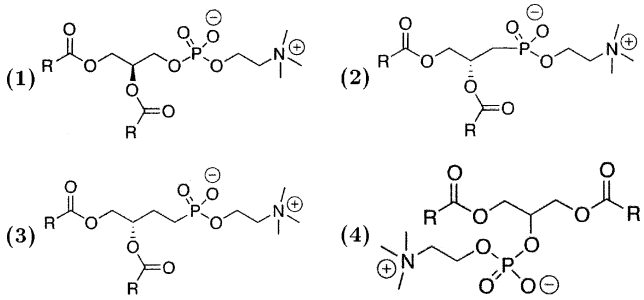

Figure 1. (1) *S*-DC(8,9)PC. (2) The *R*-"C3" DC(8,9)PC phosphonate derivative. (3) The *S*-"C4" DC(8,9)PC phosphonate derivative. (4) An achiral tubule-forming DC(8,9)PC isomer, "β-TFL".

(1) Oda, R.; Huc, I.; Schmutz, M.; Candau, S. J.; MacKintosh, F. C. *Nature* **1999**, *399*, 566−569.
(2) Georger, J. H.; Singh, A.; Price, R. R.; Schnur, J. M.; Yager, P.; Schoen, P. E. *J. Am. Chem. Soc.* **1987**, *109*, 6169−6175.
(3) Zastavker, Y. V.; Asherie, N.; Lomakin, A.; Pande, J.; Donovan, J. M.; Schnur, J. M.; Benedek, G. B. *Proc. Natl. Acad. Sci. U.S.A.* **1999**, *96*, 7883−7887.
(4) Blanzat, M.; Massip, S.; Spéziale, V.; Perez, E.; Rico-Lattes, I. *Langmuir* **2001**, *17*, 3512−3514.
(5) Selinger, J. V.; MacKintosh, F. C.; Schnur, J. M. *Phys. Rev. E* **1996**, *53*, 3804−3818.
(6) Kirsch, J. E.; Clark, N. A.; Thomas, B. N., manuscript in preparation.
(7) Thomas, B. N.; Corcoran, R. C.; Cotant, C. L.; Lindemann, C. M.; Kirsch, J. E.; Persichini, P. J. *J. Am. Chem. Soc.* **1998**, *120*, 12178−12186.

10.1021/ja040191w CCC: $30.25 **© 2005 American Chemical Society**

diameters are approximately twice that of DC(8,9)PC tubules, but whose 65.3 and 62.6 Å interlamellar spacings[7,8] closely straddle the 64.7 Å DC(8,9)PC tubule interlamellar spacing. These distances are consistent with a long-axis tilt of 32° from the membrane normal for fully extended, all-trans methylene molecular configurations, with no interdigitation, as proposed by Caffrey et al.[9] Variation of a few angstroms between intralamellar spacings of different molecules, tubules is small in comparison to the 2-fold changes in tubule diameter. Interestingly, the SAXS correlation lengths ξ, proportional to tubule wall thicknesses, is almost exactly *halved* from the DC(8,9)PC $\xi = 430$ Å to the $\xi = 210$ Å phosphonates as the tubule diameters double; force-modulation AFM shows a corresponding increase in the thinner-walled phosphonate tubules' membrane deformability.[8]

AFM also corroborates the SAXS tubule-wall thickness determinations in a more direct fashion: Phosphonate tubules deposited on glass substrates sometimes partially unravel at their ends, allowing direct AFM measurement of membrane thickness. Examination of partially unwound phosphonate tubules on flat substrates[10] shows that the flat, unraveled portions of the tubules always have heights of order ~115 Å, approximately *twice* the expected height of a single bilayer at the known $L_{\beta'}$ tilt angle of 32°.[9] (This value corresponds closely to the SAXS-determined 210 Å, for the Bessel-function model used in the SAXS data analysis accounts for *two* such layers.) Thus, phosphonate tubule walls must be composed of two bilayers, and because they are known from SAXS to be half as thick as DC(8,9)PC tubule walls, we conclude that DC(8,9)PC tubule walls are four bilayers thick.

The stringent conservation of the tubule wall's bilayer spacing is further demonstrated by DC(8,9)PC tubule-forming solutions to which a protein, lysozyme, has been added. This mixture's dominant self-assembly products are not cylindrical tubules, but gently tapered hollow *cones*.[11] SAXS shows that, like the protein-free cylinders, cones appear to consist of four bilayers spaced at 66.2 Å, very close to the intralamellar spacing of 64.7 Å for protein-free DC(8,9)PC tubules.

There is no satisfactory theoretical model describing neither these varied tubule structures nor their formation through the disparate mechanisms described earlier. In view of the highly unfavorable energetics of exposed hydrocarbon tails found along the edges of these long ribbons, the question of how ribbons possessing ~200:1 aspect ratios can form spontaneously logically precedes that of how the ribbon chiralizes and winds helically to form a closed cylinder. Another interesting tubule feature that a satisfactory theory must explain is the closely conserved ~64.7 Å interlamellar spacing observed in structures of significantly different size and symmetry. We now describe a previously unreported object, the "tubelet", which we believe to be a tubule and cone precursor, whose structure may address these fundamental questions.

The tubelet is a *flattened* hollow tube that resembles an uninflated fabric firehose of width ~1 μm. These flattened tubes have a pronounced tendency to twist or wind helically, and we assert that the phospholipid bilayer ribbon from which tubules are presumed to form is actually the tubelet. Tubelet structure addresses the ribbon-edge energetics problem by eliminating virtually all ribbon edges, and tubelet structure explains the conservation of interlamellar spacing observed over a wide range of tubule diameters and composition (e.g., DC(8,9)PC tubules, DC(8,9)PC phosphonate derivative tubules, and DC(8,9)PC + lysozyme mixture cone and tubules). Finally, the SAXS and AFM observations that tubule walls appear to have thicknesses that are multiples of two bilayers are explained quite naturally as a consequence of the structure we describe further below.

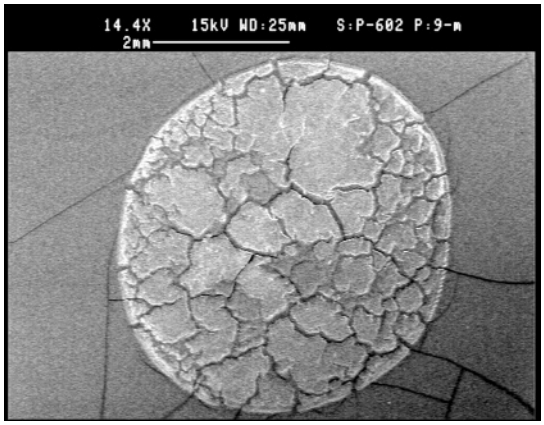

Figure 2. A low-magnification SEM image of an air-dried deposition bed of DC(8,9)PC-lysozyme specimen subjected to the tubule/cone formation thermal cycle described in the text, showing the extensive cracking of the deposition bed. This particular specimen also exhibits cracking of the substrate face; when this occurs there is no apparent registry with specimen cracking. The scale bar is 2 mm.

2. Experimental Section

The specimen protocols we employed were developed in the course of studying protein-modulated tubule formation and have been described elsewhere;[11] the salient features of those procedures are summarized here.

2.1. Specimen Preparation. 2.1.1. Thermal Cycling of Protein/DC(8,9)PC Preparations. A quantity of 1 mg of *R*-DC(8,9)PC (compound **1** of Figure 1) was dispersed in 1 mL of a 90:10 (v:v) mixture of reagent-grade ethanol and 18 M-ohm water mixture with 1 mg of lysozyme (14 kDa, from chicken egg white, Sigma Chemical). This homogeneous lipid/protein dispersion was then subjected to the standard tubule formation thermal cycle: (a) heating the dispersion to clarity (~55 °C) while stirring vigorously and then (b) cooling to room temperature at ~0.1 ± 0.02 °C/min.

2.1.2. Scanning Electron Microscopy. The protein/DC(8,9)PC precipitate and supernatant were stirred, and a drop of this homogenized sample was placed upon a conductive carbon substrate (12-mm diameter Carbon Adhesive Tabs from Electron Microscopy Sciences) and allowed to air-dry. As the specimens air-dried over the course of several hours, a network of cracks formed in the deposition bed, producing a surface resembling a dried lake bed, as seen in the low-magnification SEM of Figure 2. Protein-free deposition beds and substrates remained completely smooth and uncracked. We conjecture that the lysozyme, certainly a random coil in the 75% ethanol solution, forms a gel that contracts slightly upon desiccation, and this gel cracks in a dried "lake-bed" pattern about randomly placed contraction centers on the drying gel surface.

2.1.3. Freeze-Fracture Electron Microscopy. Freeze-fracture specimens were prepared by sandwiching the DC(8,9)PC and DC(8,9)PC/lysozyme mixtures between 2 mm × 2 mm Cu or glass planchettes and quenching them by rapid immersion in liquid propane or nitrogen.

(8) Thomas, B. N.; Corcoran, R. C.; Cotant, C. L.; Lindemann, C. M.; Kirsch, J. E.; Persichini, P. J. *J. Am. Chem. Soc.* **2002**, *124*, 1227−1233.
(9) Caffrey, M.; Hogan, J.; Rudolph, A. S. *Biochemistry* **1991**, *30*, 2134−2146.
(10) Lindemann, C. M.; Kirsch, J. E.; Clark, N. A.; Thomas, B. N., manuscript in preparation.
(11) Mishra, B. K.; Thomas, B. N. *J. Am. Chem. Soc.* **2002**, *124*, 6855−6871.

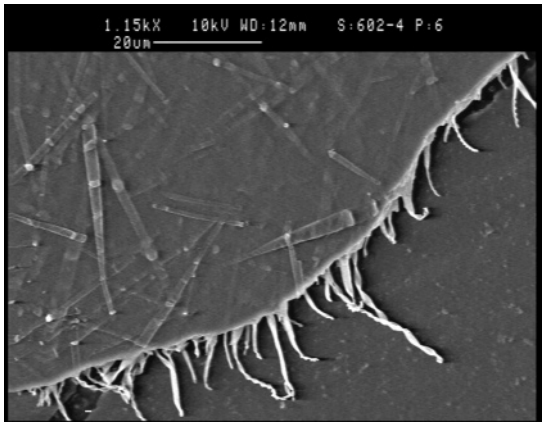

Figure 3. Top view of a protein-bearing deposition bed crack discontinuity. Cones are evident on the unbroken bed face, but tubelets are only resolvable when they emerge at the crack discontinuity face.

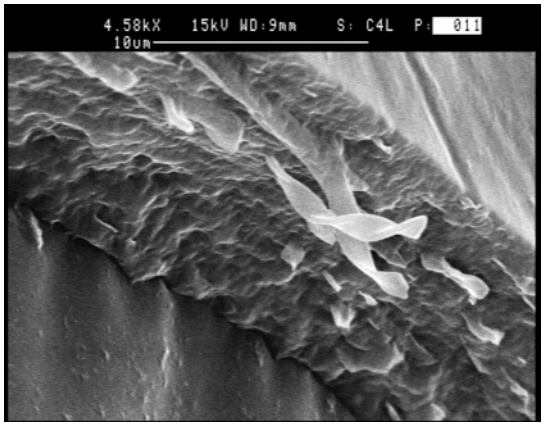

Figure 4. "Edge-on" view of a protein/tubule deposition bed crack, showing stratification and broken ribbonlike structures projecting into free space.

The specimens were fractured in cold in vacuo, and replicas were made by coating them with platinum and carbon under vacuum.

3. Results and Discussion

TEM and SEM images of the smooth face of uncracked regions of protein-bearing specimens are very similar: conically tapered tubules, possessing helical "stripe" features, are abundant. The crack discontinuities found in protein-bearing specimens, however, give unprecedented SEM access to the bed interior, and by extension, the bulk solution from which the bed forms, in a manner reminiscent of electron microscopy freeze-fracture. The principal differences are that the present case is a slow, essentially isothermal process, and that specimens may be examined directly without the need to create replicas. Another important difference is that, because the ribbonlike tubelets extend from the deposition bed into space, they are free of interfering specimen background and can be examined in great detail over substantial lengths by SEM, revealing fine structure, as shown in Figure 3. Conventional freeze-fracture does not reveal structures unambiguously resolvable as tubelets, in part because of the rather limited length scales that freeze-fracture techniques expose, while tubelets projecting from crack discontinuities may be examined for lengths of order $\sim$20 μm. Finally, the crack discontinuities permit detailed examination of the deposition bed structure normal to the substrate surface, which is central to the interpretation of our results. We now describe this structure and, in turn, the different states in which tubelets are found.

3.1. Deposition Bed Stratification. The dried protein-containing deposition bed is vertically segregated, with ribbonlike structures emerging from the crack face only at some depth from the deposition bed surface, as seen in Figure 4. We conjecture that the lysozyme/tubule mixture forms an entangled fluid matrix whose structure is determined by the interplay of three forces: gravity (sedimentation), electrostatic charge separation, and surface tension. The slow evaporation of solvent from the droplet causes it to gel, fixing these components at, or near, their equilibrium electrostatic positions. With continued evaporation the gel gradually desiccates, and as the deposition bed's volume decreases, deep cracks form perpendicular to the bed surface. It is evident from the alignment and length of the embedded ribbonlike structures that this contraction and cracking process is gentle: the ribbons are typically pulled $\sim$20 μm from the crack edge before they break. Our stratification observations are consistent with reports of sol−gel processes where stratification is characterized in terms of electrostatic charge separation energy minimization.[12] In the present case, stratification places cones and tubules at the bed surface: Neither are found at the crack interface away from the surface or found with conventional freeze-fracture probes of the bulk.

This confinement of cones and tubules to the bed surface and concurrent exclusion of ribbonlike tubelets explains why tubelets are in general unobservable by the surface-sensitive SEM and AFM probes performed on an uncracked bed surface region. Tubelets are also not discernible by TEM, because at the lipid concentrations required of these studies, the deposition bed is a dense tangle of tubules, cones, and tubelets that cannot be resolved by transmission-mode imaging. Rarely, however, a flat, untwisted tubelet is found near enough to the surface to be detected by SEM, but prior to our ability to examine crack discontinuities and resolve their structure, these structures were misinterpreted as partially submerged tubules.

3.2. Tubelets. Tubelets project roughly normal from the crack discontinuity face, consistent with the directionality that gel "lake-bed" drying is expected to create. Tubelets typically extend $\sim$20 μm from the crack face, but vary from submicrometer lengths to tubelets that emerge from one crack face, extend unbroken over $\sim$100 μm, and enter the opposing crack face. There is a weak dependence of projected tubelet length upon locale; that is, tubelets in a given region have approximately the same length. We interpret this observation as a consequence of local crack discontinuity evolution, with the shortest tubelets presumably breaking as a consequence of rapid crack separation or separation when the gel had become too solid for the tubelet to slide easily out of the crack face. Because tubelets are obscured when they enter the deposition bed, their total length is difficult to assess. Tubelets that enter the deposition cake close enough to the surface to be observed by SEM can be tracked for lengths of $\sim$30 μm before the tubelet is obscured by the deposition bed, giving a total observed length of some 50 μm. This length, in view of the observation conditions, is consistent with total tubelet lengths of order of 100 μm we expect for tubule formation.

(12) Ichinose, I.; Kuroiwa, K.; Lvov, Y.; Kunitake, T. In *Multilayer Thin Films*; Decher, G., Schlenoff, J. B., Eds.; Wiley-VCH: Weinheim, Germany, 2003; pp 155−175.

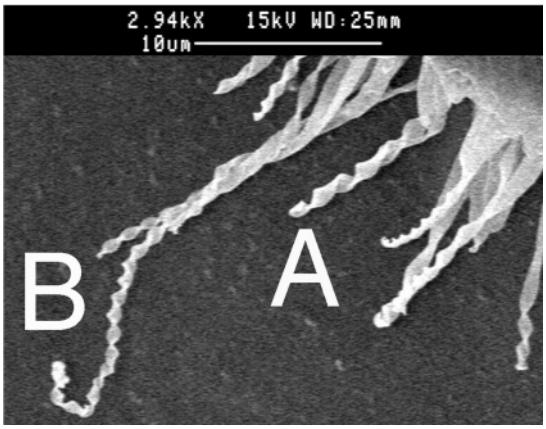

Figure 5. A crack face discontinuity from which structures possessing types "A" and "B" windings are seen to project.

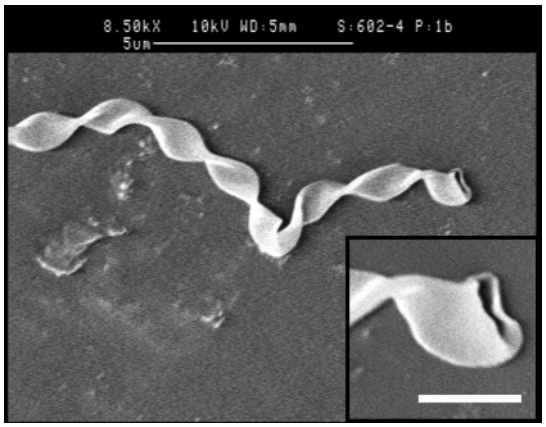

Figure 6. An axially twisted (type "B") tubelet, with characteristic ~3-μm twist periodicity and a 90° kink where axial twist handedness sometimes, but not always, changes chiral sense. (This structure's left-handed twist does *not* change chiral sense at this junction.) (Inset) Magnification of the hollow tubelet's right end. The scalebar is 1 μm.

Under our conditions tubelets are always flattened, like an uninflated fabric firehose, and either in (1) a cylindrically wound state (which we will refer to as a type "A" curvature following the notation of MacKintosh et al.[1]), (2) an axially twisted state (type "B" curvature), or occasionally, in (3) an unwound, untwisted flat state.

Axially Twisted Tubelets. The axial (type "B") winding is a twist about the structure's long axis, as shown in Figure 5, and is the dominant structure under our conditions. There is some variation in twist periodicity, but the periodicity of most axially twisted, type "B" structures is approximately 3 μm.

Cylindrically Wound Tubelets. Less common, to the extent of a few percent under our formation conditions, is the type "A" winding of the ribbon to form a cylinder-like structure, also seen in Figure 5.

Flat Tubelets. Twisted and wound tubelets typically have flat regions in their first ~1−2 μm from the crack face, which we tentatively interpret as an effect of stretching as the crack faces separate. Tubelets that remain flat over an extent of $\geq$5 μm are rare under our observation conditions. Flat tubelets are sometimes found in groups in narrow ($\leq$10 μm) cracks like that of Figure 7, which suggests local uniformity of formation conditions at the time of crack separation; perhaps these tubelets had not yet chiralized before becoming exposed and desiccated in free space.

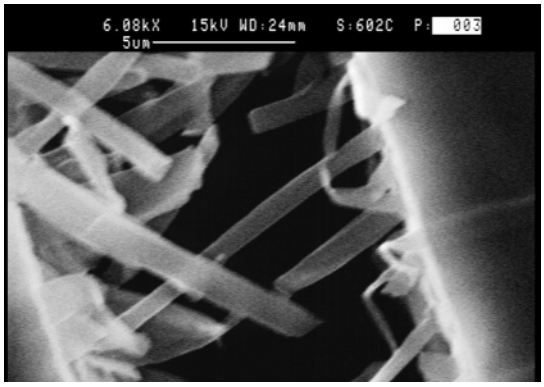

Figure 7. Unwound tubelets at a narrow crack interface.

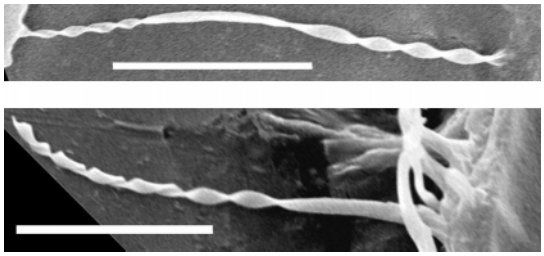

Figure 8. (Top) A tubelet that emerges from a crack face discontinuity with a right-handed type "B" winding, changes to flat configuration at its center, and resumes a right-handed type "B" winding before emerging at the opposing crack face discontinuity. (Bottom) A tubelet that undergoes a continuous transition from a type "A" winding at its left, to a type "B" winding at its center, and finally to a flat state as it enters the crack face discontinuity. Both scalebars are 10-μm long.

Transitions between flat, axial, and cylindrical regions are common, as seen in Figure 8. The twist or winding's chiral sense sometimes, but not always, changes at "A"/"B", flat/"A", or flat/"B" junctions. Another common transition, the "B"/"B" kink, is seen in Figure 6; here too, the twist's chiral sense often, but not always, reverses.

Current theoretical treatments of tubule structure account for the helical curling of the bilayer ribbons by combining molecular tilt and intrinsic molecular chirality. Because chirality imparts a tendency for director twist or bend, a consequence is that a bilayer patch composed of tilted molecules will not be flat but instead saddle-shaped in its ground state. Thus, the helical shape of the tubules $L_{\beta'}$ ribbons has been presumed to arise from such a bilayer twist. Several aspects of one such theory, developed to describe a system composed of achiral gemini surfactant ribbons that undergo helical twist in proportion to the enantiomeric excess of a chiral counterion,[1] are relevant to our system. We now extend this theory's predictions to our hollow bilayer tubes.

Specifically, our observations strongly suggest the process illustrated in Figure 9: The formation of a continuous hollow bilayer tube, the tubelet, which spontaneously flattens in either an axial (type "B") curvature, a cylindrical (type "A") curvature, or far less commonly, with no curvature. Because of their size and helical pitch, we interpret the cylinders resulting from type "A" winding to be tubules. *That is, we believe phospholipid tubules and DC(8,9)PC/lysozyme cones are actually the helical winding of tubelets.* This model explains quite naturally several fundamental tubule features.

First, the highly unfavorable solvation energy cost along the ribbon's edges is eliminated or, more properly, replaced by the

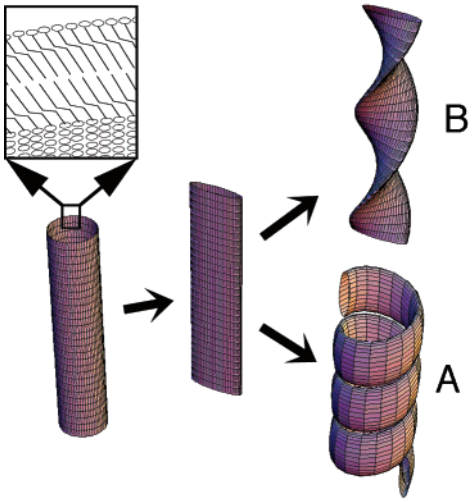

Figure 9. Formation of types "B" and "A" curvature structures appears to begin with the formation of the cylindrical tubelet (left), which spontaneously flattens (center). The tubelet occasionally remains flattened but far more likely assumes a type "B" curvature conformation (top right) or a cylindrical "A" curvature (bottom right). The inset drawing indicates the bilayer orientation of the amphiphilic molecules.

energetics of the sharp curvature occurring at the flattened tube's creases. We speculate further that such creases may be a manifestation of membrane chiralization. MacKintosh et al.[1,5] and Kamien and Selinger[13] have advanced the idea that chiral defect lines must form in sufficiently large chiral domains, and we speculate that as tubelets lengthen and chiralize, their diameter, their twist, and/or winding may be determined by the energetics of frustrated chiral line defects. In any case, our experimental findings suggest evaluation of the ribbon edge/tubelet crease as a tubule feature may be fruitful.

Second, the persistence of the so-called "barber-pole" ridge on tubule surfaces and the apparent stability of DC(8,9)PC/propanol helices[2] and DC(8,9)PC phosphonate derivative helices[7,8] are also explained by this model: The ridges are not an "edge-to-edge" meeting of two membranes, which might be expected to fuse seamlessly, but rather, the junction of two hydrophilic membrane faces. Under this model, the "open" helices found in 2-propanolic DC(8,9)PC systems or phosphonate DC(8,9)PC derivative systems do *not* present exposed hydrocarbon along their long edges but, rather, more stabilized hydrophilic headgroups.

A third tubule feature that is explained by the proposed tubelet substructure is the remarkably tightly conserved interlamellar spacing found in structures of different composition, dimensions, and in the case of cones, symmetry. This conservation can be understood in terms of the structure we propose to be common to them all, the collapsed, helically wound tubelet. Finally, the SAXS and AFM determinations that DC(8,9)PC and phosphonate tubule walls are either two or four bilayers thick are also easily explained if the postulated bilayer ribbon is actually a collapsed bilayer tube. Under this model, the tubule of Figure 5 is expected to have a wall thickness of two bilayers, and tubule wall thicknesses can be incremented only by multiples of two bilayers, consistent with SAXS and AFM determinations.

The gemini surfactant/bilayer ribbon theory differentiates strongly between type "A" and "B" curvatures: For a fluid membrane, cylindrical curvature—either as a complete tubule or as a helical ribbon precursor to a tubule—is not expected, but in contrast, solidlike ordering in the membrane strongly favors cylindrical curvature. The apparently continuous transitions between type "A" and "B" curvatures we observe suggest either that solid/fluid assignments to tubelets are inappropriate or that the solid-to-fluid transition is not first-order in our system (e.g., perhaps as a consequence of a protein concentration gradient). This theory also predicts that ribbons may not grow beyond a certain preferred width W, and the ribbon twist period T and ribbon width W ratio T/W is expected to be of the order of 1, consistent with our findings. Also, the type "B" configuration (axial twist) is predicted to be energetically favored for ribbons, consistent with the preponderance of type "B" windings in our tubelet populations. Taking the simplest possible view that our observations are representative of the equilibrium state and that only a few percent of tubelets are in the type "A" configuration, one could naively estimate an energetic difference greater than $\sim 2kT$ per length between "A" and "B" configurations. This simple picture is quickly complicated by the comparatively large number of tubelets that have transitions between axial, cylindrical, and flat regions within a few micrometers along their lengths, suggesting a substantially lower energy difference between tubelet configurations. While it appears clear that the "B" twist is energetically lower, deconvolving tubelet winding energetics from formation kinetics will present a substantial experimental challenge.

Are tubelets a protein-induced morphology unrelated to tubule formation? While the appearance and dimensions of the tubelet type "A" helical windings of Figure 5 and the bottom of Figure 8 argue powerfully for tubelets being a tubule precursor, tubelets (and cones) have been observed only in protein-containing specimens. We nevertheless argue that tubelets are tubule precursors in protein-free preparations as well, but that they are unobservable by conventional SEM and TEM in such specimens.

SEM and TEM of the uncracked regions of protein-containing specimens, like that of the top portion of Figure 3, show the coexistence of cones and tubules, and neither probe detects tubelets in these smooth regions. Nevertheless, tubelets *are* present in great numbers, as seen at the crack discontinuity at the bottom of Figure 3. SEM fails to detect tubelets in uncracked deposition regions because the deposition bed's stratification places them away from the surface, and TEM is incapable of resolving tubelets because of the dense jumble of structures found along the $\sim$12-μm deposition bed depth. But, at deposition bed crack discontinuities, which happen to occur only in protein-containing specimens, tubelets *are* seen, and they can be examined by SEM free of interfering specimen background over substantial distances. The unexpected circumstance under which tubelets are seen (i.e., only at crack face discontinuities) compels us to consider that tubelets are also present in protein-free specimens, but are unobservable because protein-free specimens do not crack to reveal the deposition bed interior. Such discontinuities in protein-free specimens would permit direct comparison of the beds' internal organization and of these long structures. But vertical slices made into these deposition beds do nothing to reveal the tubelet's long structure and create such large artifacts as to render the specimen uninterpretable, and conventional freeze-fracture's loss of orientational information

(13) Kamien, R. D.; Selinger, J. V. *J. Phys.: Condens. Matter* **2001**, *13*, 1−22.

and limited length scale render it similarly ineffective in studying tubelets in either protein-bearing or protein-free specimens.

Optical video microscopy shows great similarities between tubule and cone formation, and SEM and SAXS examinations of their internal structures further strengthen the notion that cones and cylinders must be considered to be more alike than different. The salient tubule and cone features that are explained by a tubelet substructure, for example, the persistence of exterior helical ridges, the tight conservation of interlamellar spacing, and the DC(8,9)PC-related systems' tubule wall thicknesses are integral multiples of two bilayers make the interpretation that tubelets are cone and tubule precursors more compelling. We therefore assert that tubelets *are* involved in regular, protein-free DC(8,9)PC systems and that the wholly unexpected crack discontinuities in the protein-containing specimens have merely permitted unprecedented access to the solution interior that contains them.

4. Conclusion

The complex interplay of gravity, electrostatic charge, and surface tension determines the structure of the entangled protein-laced fluid matrix that subsequently gels, dries, cracks, and fortuitously exposes the structure we call the "tubelet". These structures appear to be tubule precursors and are topologically distinct from the bilayer ribbons from which tubules have been assumed to form. Tubelet structure explains several salient tubule features (e.g., the extraordinarily high aspect ratio of the structure wound to make tubules) and may represent a major shift in our understanding of tubule structure and formation. The potential utility of tubules in applications such as biomedical encapsulation should be reconsidered as well: Rather than presenting a comparatively simple, 0.5-μm-bore cylinder, tubules should now be considered a secondary winding of a smaller tube that may offer encapsulant retention times substantially longer than that expected from the simple cylinder.

Acknowledgment. B.N.T. was supported by NSF CAREER Grant CHE-0096330. C.D.C. was supported by NSF IGERT DGE-9987603, a Louisiana Economic Development Assistantship, and an LSU Coates Research Travel Award. We thank Ms. Cindy Henk of the LSU Biological Sciences Department and Dr. J. C. Jiang of the LSU Mechanical Engineering Department for their expert technical assistance and guidance in the scanning and transmission-mode electron microscopy, respectively. We also thank Fred MacKintosh of the Vrije Universiteit Amsterdam Department of Physics for helpful discussions and Noel Clark of the University of Colorado Physics Department for the use of freeze-fracture equipment.

JA040191W